Detection and Interpretation of Left-Moving Severe Thunderstorms Using the WSR-88D: A Case Study

JOHN W. NIELSEN-GAMMON

Cooperative Institute for Applied Meteorological Studies, Texas A&M University, College Station, Texas

WILLIAM L. READ

Houston Area National Weather Service Office, NOAA, League City, Texas

(Manuscript received 4 January 1994, in final form 23 August 1994)

ABSTRACT

Left-moving supercells, which rotate anticyclonically, are much less common than their right-moving counterparts but are nevertheless capable of producing severe weather. On 26 May 1992, a severe left-moving thunderstorm over east Texas developed within range of the WSR-88D (Weather Surveillance Radar-1988 Doppler) radar at League City, Texas. The evolution of the left-moving thunderstorm, including its split from its parent thunderstorm, is presented using standard WSR-88D products. The storm produced wind damage and large hail, whose presence in the thunderstorm caused a flare echo in the return signal. No automated WSR-88D algorithms exist to detect mesoanticyclones or flares, so the subjective interpretation of these radar signatures as indicators of severe weather can be critical for the proper issuance of warnings for such storms.

1. Introduction

In the typical life cycle of a long-lived, severe thunderstorm, a rotating supercell evolves from a multicell thunderstorm (Lemon and Doswell 1979; Bluestein 1993). The source of the rotation is low-level vertical wind shear, which when ingested into the updraft produces a maximum/minimum couplet in the vertical component of vorticity (Rotunno 1981). This process can cause a single storm to split, as shown in Fig. 1, producing a cyclonically rotating supercell moving to the right of the mean midlevel winds and an anticyclonically rotating supercell moving to the left of the mean midlevel winds (Weisman and Klemp 1986). In a typical supercell, this rotation is manifested as a *mesocyclone*, a 5–10-km-diameter vortex in quasi solid body rotation, which forms at midlevels within the updraft of the storm. When the sense of rotation is anticyclonic, the feature is called a *mesoanticyclone* (e.g., Davies-Jones 1986).

The most common scenario in the central United States is for the right-moving supercell to remain intense and the left-moving supercell to weaken or fail to develop. This tendency has been shown by extensive investigation (Klemp and Wilhelmson 1978; Davies-Jones 1984; Brandes 1984) to be a direct consequence of the typical wind shear profile. When the wind shear vector rotates clockwise with height (e.g., with southerly winds at low levels and progressively stronger westerly winds at mid and upper levels), the right-moving storm is favored. If the wind shear vector rotates counterclockwise, a much rarer occurrence in convective environments, the left-moving storm is favored. If the wind shear is unidirectional, numerical simulations produce the mirror-image supercells shown in Fig. 1, with the anticyclonic supercell moving left of the direction of the midlevel wind and the cyclonic supercell moving right of the direction of the midlevel wind.

Operational severe weather nowcasting and short-range forecasting is being revolutionized in the United States by the installation of the NEXRAD system of Doppler radars at National Weather Service offices and military installations across the country (Crum and Alberty 1993; Alberty 1993). The formal name for each radar is Weather Surveillance Radar-1988 Doppler, or WSR-88D. Thunderstorm mesocyclones and mesoanticyclones are manifested on Doppler velocity scans by a storm-relative inbound–outbound couplet in radial velocity about 5–10 km across (Donaldson 1970; Burgess 1976). The detection of mesocyclone signatures has been automated on the WSR-88D as one of many severe weather detection algorithms. The WSR-88D is also capable of tracking individual thunderstorm cells and computing and plotting storm motion. Another algorithm checks for the existence of a tornadic vortex signature (TVS) within a previously identified mesocyclone.

Corresponding author address: Dr. John W. Nielsen-Gammon, MS 3150, Dept. of Meteorology, Texas A&M University, College Station, TX 77843-3150.

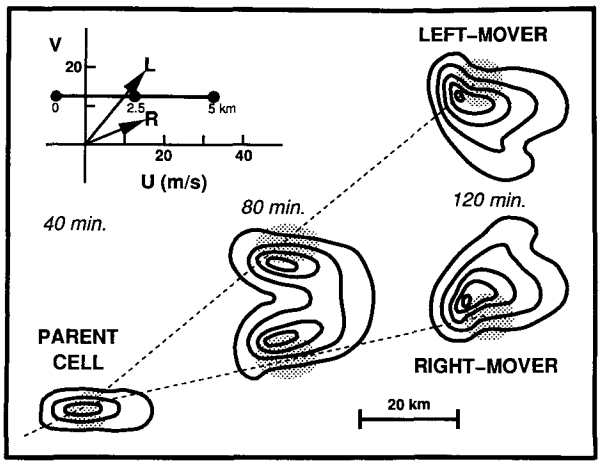

FIG. 1. Numerical simulation of a splitting storm, shown at 40, 80, and 120 min into the simulation. The environmental hodograph, at upper left, consists of unidirectional shear. The split produces two mirror-image supercells, one moving to the right of the environmental shear (R) and one moving to the left of the environmental shear (L). Storm structure is indicated by rainwater fields at 1.8 km (analogous to low-level reflectivity), contoured every 2 g kg^{-1}. Updrafts at 4.6 km exceeding 5 m s^{-1} are shaded. Redrawn from Weisman and Klemp (1986).

The WSR-88D mesocyclone detection algorithm ignores mesoanticyclones (Zrnić et al. 1985). In those instances where the shear favors anticyclonically rotating thunderstorms or is unidirectional, the radar operator must identify and monitor left-moving thunderstorms manually and be alert for possible mesoanticyclone formation.

Few anticyclonic supercells have been documented in the literature. Browning (1968) described left-moving supercells as mirror images to right-moving supercells and noted that they were less common, but did not quantify their relative frequency. Burgess (1981) and Davies-Jones (1986) report that mesocyclones outnumber mesoanticyclones by about 50 to 1 in NSSL-observed storms, and that none of the mesoanticyclones were associated with tornadoes. The two storms with mesoanticyclones examined in detail by Burgess (1981) were produced by classical storm splitting, occurred with unidirectional environmental shear, and persisted for less than 45 min. Houze et al. (1993) report that of 18 severe hailstorms observed in Switzerland between 1975 and 1982 possessing a hook echo indicative of supercells, 5 were left movers with radar patterns indicating anticyclonic rotation. Possibly the most completely documented anticyclonically rotating thunderstorm was a long-lived cell that formed within dual-Doppler range in Colorado (Knupp and Cotton 1982a,b) and which was simulated successfully by a three-dimensional cloud model (Tripoli and Cotton 1986). The storm environment featured a hodograph that curved anticyclonically with height, and the left-moving, anticyclonic cell became the dominant updraft. With the ongoing installation of WSR-88D radars across the country, additional cases of severe or long-lived left-moving thunderstorms are being identified and examined (Andra 1993; Kleyla 1993).

This paper discusses one case of a left-moving thunderstorm observed with the WSR-88D located at the Houston Area National Weather Service Office (WSO) in League City, Texas. The thunderstorm occurred on 25–26 May 1992 and went through a typical supercell life cycle. The storm produced severe weather in the Texas towns of Coldspring and Livingston. See Fig. 2 for the track of the storm and the locations of places mentioned in the text.

In this paper, an overview of the environment of the storm (henceforth called the Coldspring storm) is followed by a detailed chronology of the storm as seen in standard products of the WSR-88D. Because radar data were not yet being archived at the WSR-88D site, information on the storm is limited to the products that were generated in real time. Brief descriptions of the WSR-88D products are contained in Klazura and Imy (1993). Because many of the WSR-88D algorithms are not designed to detect such a storm, this description concentrates on features that a radar operator can use as indications of rotation and severity using base velocity and reflectivity products.

All times in this article are in UTC. To obtain Local Standard Time, subtract 6 h from the given times. The date, except where noted, is 26 May 1992.

2. The severe storm environment

The Coldspring storm formed in an environment of weak large-scale forcing. The nearest 500-mb vorticity maximum was over Missouri (not shown). At the surface, a cold front had moved into Texas from the north and weakened, leaving a broad north–south temperature and dewpoint gradient in the area. Surface observations, plotted in Fig. 2, show predominantly southerly flow at coastal stations, possibly aided by a seabreeze circulation, while winds farther inland were comparatively disorganized and most commonly northeasterly. Surface dewpoints in the area of storm formation were near 20°C.

A visual inspection of nearby observations suggests that the Coldspring storm formed in a region of mesoscale convergence. To quantify and understand the convergence pattern, a Barnes univariate objective analysis was performed on the observed winds, using the default analysis parameters determined by GEMPAK (Koch et al. 1983). The analyzed divergence field (Fig. 3) includes a convergence maximum of greater than 8×10^{-5} s^{-1} in the area in which the Coldspring storm formed. The overall pattern includes a long band of convergence parallel to the coast, suggestive of a sea breeze. The reason for the maximization of convergence in the area of the storm, which would have contributed to its rapid formation and the subsequent development of other cells in the area, is not known.

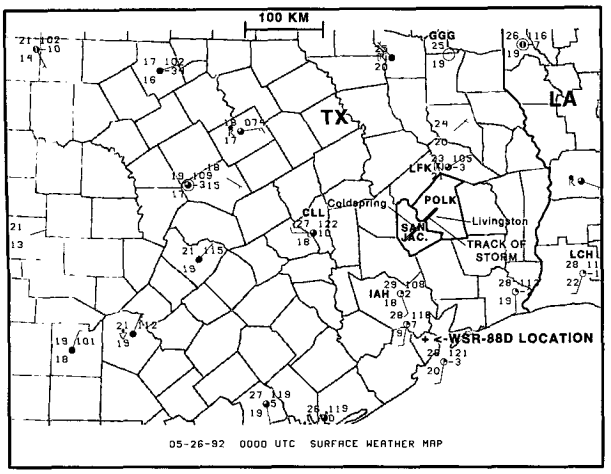

FIG. 2. Surface weather map for southeast Texas and southwest Louisiana at the time of formation of the severe left-moving thunderstorm. The location of the radar, nearby weather stations and sounding sites, the track of the storm, and the counties in which severe weather occurred are shown. A standard station model is used, with (clockwise from upper left) temperature (°C), present weather (if any), dewpoint temperature (°C), three-hour pressure change (tenths of mb), and pressure (tenths of mb, leading "10" dropped). Sky condition and winds are also standard, with one long barb equaling 5 m s^{-1}.

The closest 0000 UTC soundings (Fig. 4), from LCH (Lake Charles, Louisiana) and GGG (Longview, Texas), favor convection and suggest the possibility of some severe convection. Both soundings were relatively moist and possessed convective instability (convective available potential energy at LCH = 2440 J kg^{-1}, at GGG = 1034 J kg^{-1}; lifted index at LCH = −6, at GGG = −4) with little inhibition to convection (convective inhibition at LCH = 11 J kg^{-1}, at GGG = 45 J kg^{-1}) and moderate shear (bulk Richardson number at LCH = 97, at GGG = 27). Since bulk Richardson numbers below 50 are associated with multicell or supercell thunderstorms (Weisman and Klemp 1982), the soundings at LCH and GGG and the presence of

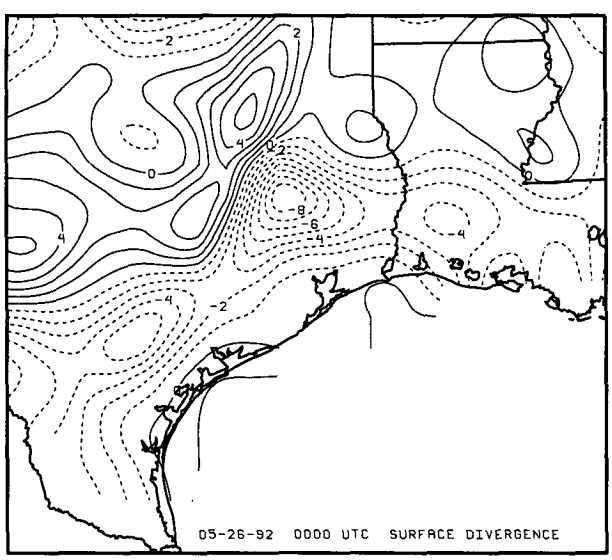

FIG. 3. Analyzed surface divergence (contour interval 1 × 10^{-5} s^{-1}; convergence dashed) for same time as in Fig. 2.

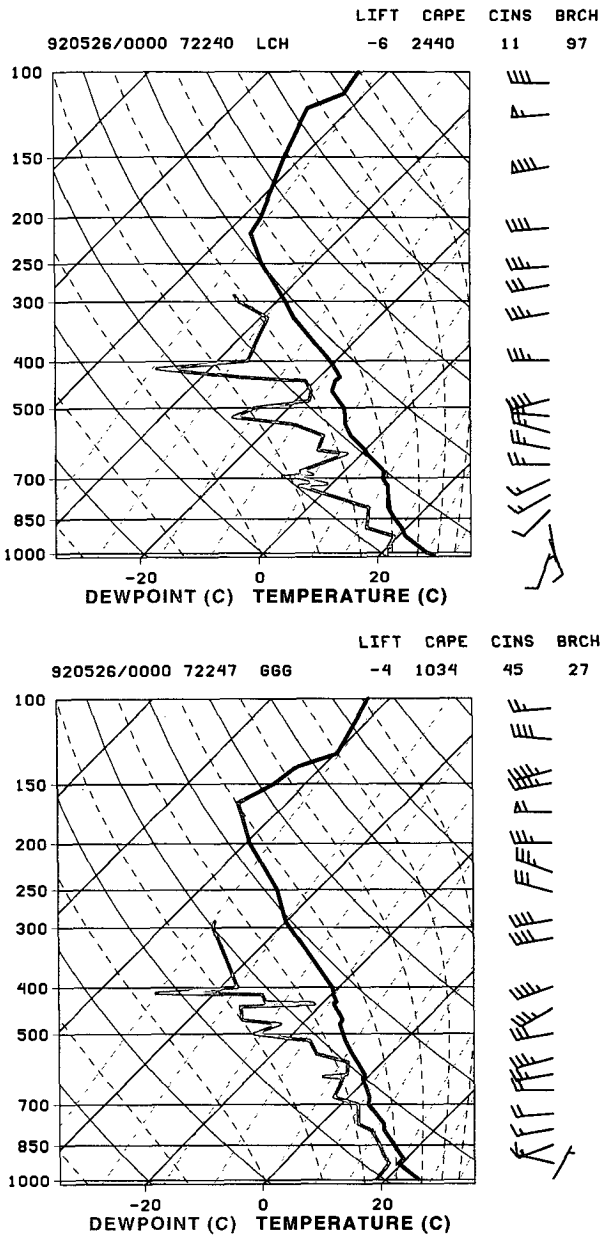

FIG. 4. Skew T–log$p$ sounding diagrams for Lake Charles, Louisiana (LCH), and Longview, Texas (GGG), 0000 UTC 26 May 1993. Solid lines are temperature and dewpoint temperature, both in degrees Celsius. Pressure (vertical axis) is labeled in mb. Wind speeds are plotted in knots, with one long barb equal to 10 kt (5.1 m s^{-1}). Plotted stability indices are lifted index (LIFT), convective available potential energy (CAPE), convective inhibition (CINS), and bulk Richardson number (BRCH).

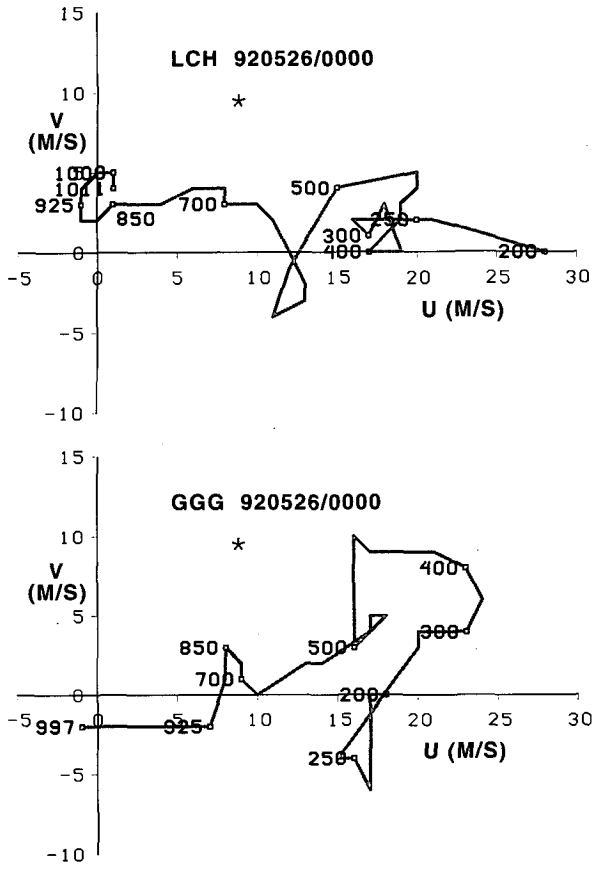

FIG. 5. Hodographs from Lake Charles, Louisiana (LCH), and Longview, Texas (GGG), 0000 UTC 26 May 1993. Wind speeds (u component along x axis, v component along y axis) are in m s^{-1}. Mandatory pressure levels are given in mb. The velocity of the Coldspring storm is indicated by the star.

low-level convergence implied widespread convection, with some convection possibly developing into supercells.

The hodographs from GGG and LCH (Fig. 5) did not show the clockwise turning of the vertical wind shear vector common to central plains severe weather environments. At LCH, the shear vector rotated counterclockwise in the lowest 100 mb, before becoming purely westerly between 900 and 700 mb. The low-level wind variations at LCH were attributable to a late afternoon sea breeze. At GGG, there was a pronounced anticyclonic turning of the hodograph from the surface to 850 mb, and a broader turning between the surface and 500 mb. Numerical simulations of supercell thunderstorms (e.g., Klemp and Wilhelmson 1978) indicate that left-moving, anticyclonically rotating supercells are favored when the hodograph turns counterclockwise, as it did at GGG, and that left-moving and right-moving thunderstorms are equally favored when the hodograph is nearly straight, as it was at LCH. Taken together, the two soundings imply a slight environmental preference for anticyclonically rotating thunderstorms in east Texas at 0000 UTC.

With the WSR-88D, vertical wind structure can be estimated in real time using the VWP (Velocity Azimuth Display Wind Profile) product (Klazura and Imy 1993), which presents a time–height cross section of horizontal winds (Fig. 6). The VWP estimates are useful as local measures of wind shear and as indicators of rapid changes in the vertical wind structure. We have found that caution must be used at League City when the returns are from clear air in spring or fall because of the likelihood that they are produced in part by migratory birds or insects. Comparisons with collocated rawinsonde observations taken during the springs of 1992 and 1993 suggest a consistent overestimate of wind speeds of 5–10 m s^{-1}, with little directional error, during the early evening. By late May, the bird migration has typically passed the upper Texas coast, so in this instance, the wind speed magnitudes were likely to be correct. The observed winds indicated a low-level backing of the wind below 4000 ft (1.3 km), implying a counterclockwise turning of the hodograph consistent with LCH and GGG and confirming the possibility of left-moving thunderstorms.

3. Evolution of the Coldspring storm

a. Initial indications of severity

Of the thunderstorms that formed within the Houston Area WSO area of responsibility that evening, only

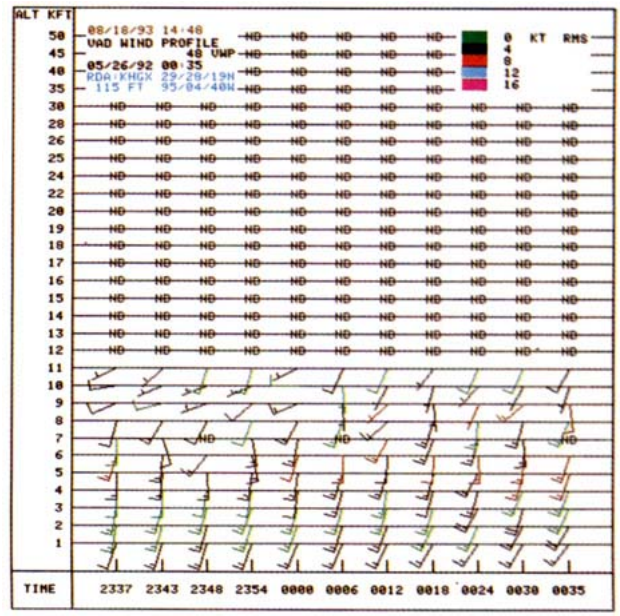

FIG. 6. VAD wind profile (time–height cross section) from the Houston Area WSR-88D, 2337 UTC 25 May 1993 to 0035 UTC 26 May 1993, showing low-level backing of wind with height. Winds are plotted using the standard model, with one long barb equaling about 5 m s^{-1}. Heights are in thousands of feet (or multiples of 305 m). ND indicates no data.

the Coldspring storm developed supercell characteristics. The storm was isolated (except for the remnants of its parent storm and short-lived right mover) for most of its life cycle, although numerous other thunderstorms were present to the north and west. The 2.0-km (1.1 nautical mile) resolution base reflectivity product from the WSR-88D for 0041 26 May (Fig. 7) shows that the thunderstorms formed a broad band across Texas into Louisiana. The Coldspring storm did not appear particularly suspicious in the large-scale reflectivity field. Although the Weather Service personnel on duty did not have the luxury of focusing on a single storm, we shall concentrate on the Coldspring storm from the development of rotation to its eventual collapse. This storm was the only storm to produce confirmed severe weather, and was also the only storm in Fig. 7 that appeared to have the structure of a supercell.

The diagnostic that first drew attention to the Coldspring storm was the Vertically Integrated Liquid-Water Content (VIL) product (Greene and Clark 1972; Winston and Rasmussen 1989), which indicated that the storm had high reflectivities distributed over a large depth of the atmosphere. Vertically integrated liquid water has been shown to be a valuable indicator of severe thunderstorms (Winston and Ruthi 1986). The time series of maximum VIL values for the storm (Fig. 8) shows a rapid increase in VIL between 0012 and 0035. (The other quantities plotted in Fig. 8 are discussed in section 3f.) At the Houston Area WSO on 26 May, this rapid increase in VIL was the primary motivation for the issuance of a severe thunderstorm warning at 0030. The storm reached a maximum computed VIL of 79 kg m^{-2} at 0035. It should be noted that at this range from the radar (125 km), WSR-88D

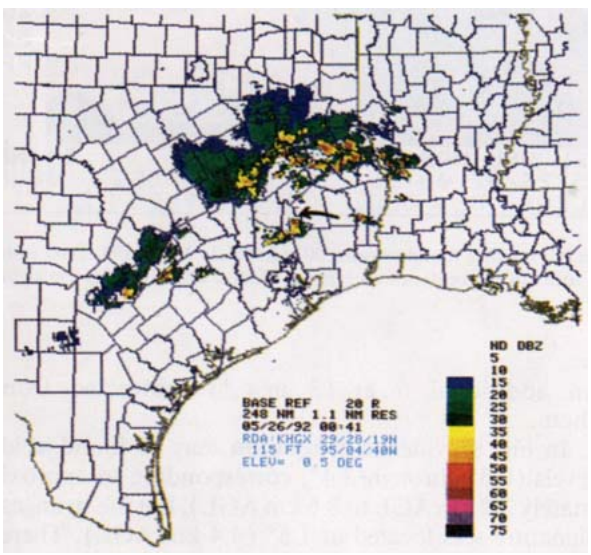

FIG. 7. Base reflectivity (in dBZ, scale to right) from the 0.5° scan of the Houston Area WSR-88D, 0041 UTC 26 May 1993. Area shown is roughly equal to that depicted in Fig. 3. The Coldspring storm is indicated by the arrow.

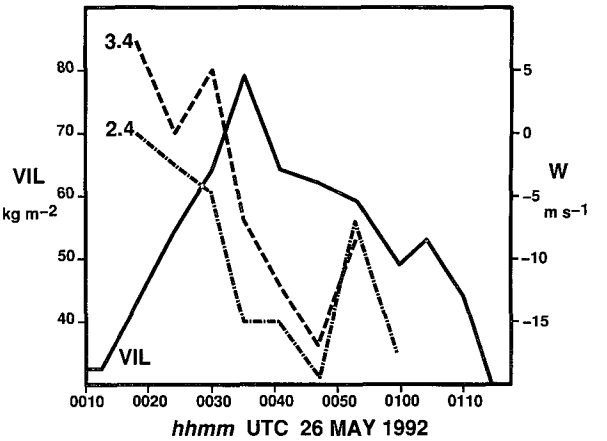

FIG. 8. Time history of maximum vertically integrated liquid water (VIL, solid) and estimated reflectivity core hydrometeor vertical velocities (dashed from flares at 3.4°, dash–dot from flares at 2.4°; see section 3f) within the left-moving thunderstorm.

VIL values are subject to overestimates of 5 to 12 kg m^{-2} (Mahoney and Schaar 1993). During the following 45 min, the VIL gradually decreased, eventually dropping below values of surrounding nonsevere thunderstorms at 0116.

Another indication that the Coldspring storm was different from its neighbors was its anomalous motion. Radar loops showed that the storm was moving to the left of and faster than other cells in the area. Based upon the motion of the reflectivity core during its lifetime, the storm's average velocity was 13 m s^{-1} (25 kt) from 223°. This storm motion is plotted in Fig. 5 and deviates strongly from the low- and midlevel winds seen in the LCH and GGG soundings.

Storm-relative environmental helicity (Davies-Jones et al. 1990) will be negative when storm motion is significantly to the left of the environmental hodograph. The most negative storm-relative helicity, -78 m^2 s^{-2}, is found in the GGG sounding. The magnitude of the helicity is much less than the threshold estimated by Davies-Jones et al. (1990) for mesocyclone formation based on observational data, or the magnitude required for numerically simulated mesocyclones (Droegemeier et al. 1993). The actual environmental helicity in the vicinity of the Coldspring storm is uncertain because of the lack of nearby soundings, the lack of nearby surface stations, and the wide differences among surface winds at surrounding surface stations. If the storm's environment was represented by the northeast wind at Lufkin (LFK), the storm-relative environmental helicity would have been much greater than the helicity estimated from the GGG sounding.

b. Radial velocity

The most dramatic storm-relative radial velocity patterns are found at 0035 (Fig. 9). The Coldspring

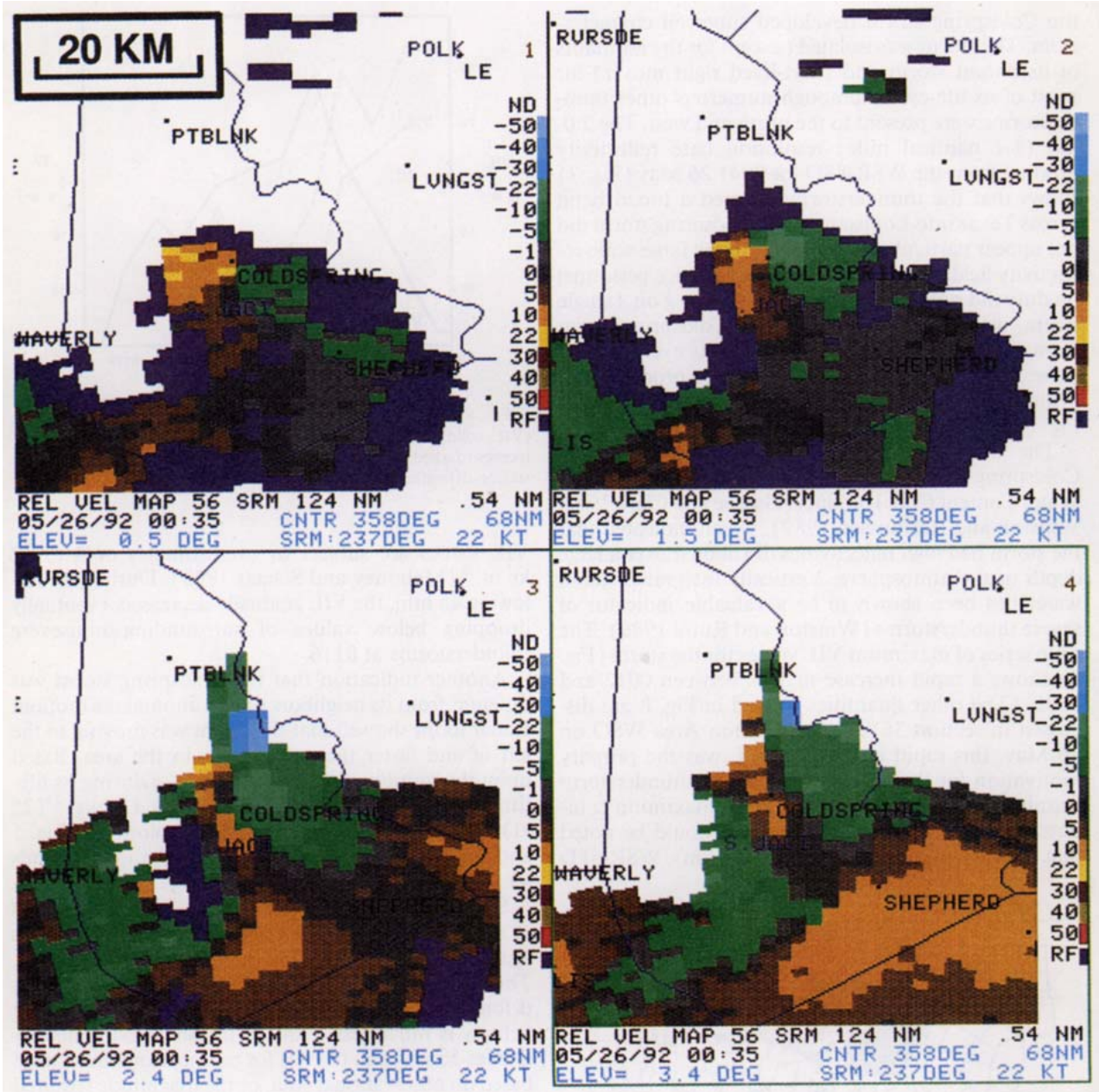

FIG. 9. Four-panel storm-relative radial velocity fields centered on the left-moving thunderstorm, 0035 UTC 26 May 1993. Data from the lowest four elevation angles are shown. The radar is located 122 km south of the center of each panel. Radial velocity scales (on right) are in knots (1 kt = 1.93 m s^{-1}).

storm is located near the center of each frame. Storm-relative radial velocities are shown here instead of raw radial velocities because they are commonly used operationally to aid in the detection of rotation and divergence patterns. The velocity used by the WSR-88D for storm motion, 22 kt (11 m s^{-1}) from 237°, differs from our estimated motion of the Coldspring storm of 25 kt (13 m s^{-1}) from 223°. If our estimated storm motion had been used, all radial velocities in Fig. 9 would have had an additional 6 kt (3 m s^{-1}) subtracted from them.

In Fig. 9 evidence of rotation may be found at all levels (0.5° through 3.4°, corresponding to approximately 2.2 km AGL to 8.6 km AGL), but the strongest signature was located at 1.5° (4.4 km AGL). There, the eastern side of the core of rotation is marked by light green shading, indicating storm-relative flow toward the radar between 22 and 30 kt (11–16 m s^{-1}). Just west of the maximum approaching flow are the

strongest receding velocities (yellow) in the convective area, with storm-relative flow between 22 and 30 kt (11–16 m s^{-1}) away from the radar. With the boundary between the two regions oriented north–south, parallel to the direction to the radar, the pattern possesses the characteristics of an anticyclonic mesovortex (Brown and Wood 1991). The centers of the range gates with the largest approaching and receding velocities are about 5 km apart, implying a local shear of -5.4×10^{-3} s^{-1} and a "Doppler angular momentum" (Zrnić et al. 1985) of -134.0×10^{-3} m^2 s^{-1}. For comparison, the WSR-88D mesocyclone detection algorithm requires that a "low momentum" mesocyclone have shear greater than 4×10^{-3} s^{-1} and Doppler angular momentum greater than 50×10^{-3} m^2 s^{-1} (Federal Meteorological Handbook 1991). Anticyclonic shear is found at all four levels and is vertically correlated. If the WSR-88D possessed a mesoanticyclone algorithm analogous to its mesocyclone algorithm, it may well have identified this feature as a mesoanticyclone.

At 2.4° (6.5 km AGL), the magnitude of the inbound/outbound couplet was just as large as at 1.5° but the area of rotation was broader, implying a weaker vorticity but a stronger circulation. Stronger approaching radial velocities extend north from the main body of the storm. These stronger velocities are biased and are discussed later. At 3.4° (8.6 km AGL), the localized anticyclonic shear was weaker but still clearly present. Finally, at 0.5° (2.3 km AGL), the scan closest to the ground, the strong anticyclonic shear may still be part of a mesovortex, but a symmetric vortex signature is lacking because the inbound (eastern) side of the possible couplet is in an area with insufficient returned signal (white) or range-obscured velocities (purple). The earth-relative radial winds at 0.5° (not shown) were strongest at this time, and this scan was probably coincident with damaging winds in Coldspring, located almost directly beneath the mesoanticyclone. One half hour after this scan, the National Weather Service received a report from the sheriff of San Jacinto County of trees and power lines downed by strong winds in Coldspring. If the damage did occur at 0035, the issuance of a warning for the Coldspring area by the National Weather Service preceded the damage by 5 min.

c. *Other indications of supercell structure*

In addition to rotation and high winds, other evidence of severity can be discerned from the reflectivity pattern. The most dramatic structures are found a few minutes later in the storm's evolution, at 0041 (Fig. 10), which resembles a classic mature supercell. An anticyclonically rotating, left-moving supercell is the mirror image of the more familiar right-moving supercell (see Fig. 1). The inflow air is to the north and northeast of the storm; the strongest reflectivities are found on the northwest portion of the storm; and the inflow notch and weak echo region are along the northern edge of the high-reflectivity core.

According to Weisman and Klemp (1986; see also Ray 1990), the features that uniquely identify a cyclonic (anticyclonic) supercell are 1) an elongation of reflectivity in the direction of the vertical wind shear; 2) a maximum gradient in the reflectivity field along the right rear (left rear) flank; 3) a several-kilometer overhang of midlevel reflectivity in the region of storm inflow, resulting in a vault or weak echo region along its right (left) flank; 4) storm motion that deviates to the right (left) of the mean wind; 5) a hooklike echo structure at the storm's right rear (left rear) flank; and 6) a mesocyclone (mesoanticyclone), first observed at midlevels, which extends in time both upward and downward. These distinguishing features develop over an hour to an hour and a half. The mesovortex (point 6) is probably the most important element in the list; a persistent (at least a few tens of minutes), deep (several kilometers) mesovortex is viewed by Doswell and Burgess (1993) as the defining element of a supercell.

The Coldspring storm, as seen in Figs. 9 and 10, possessed all of these characteristics. At 0.5°, the high-reflectivity core, elongated in the along-shear direction, had a concave indentation along its northern edge. Above this area of weak echo, the 2.4° scan had reflectivities of 50–66 dBZ, making a pronounced overhang over the weak echo region. (Storm propagation and the time interval between successive elevation angles accounts for about a quarter of the overhang.) Also at this level, a strong reflectivity gradient was present along the northern and western edges of the core. The 0.5° scan exhibited a low-level hooklike appendage according to the classification system of Forbes (1981). The mesoanticyclone and deviant cell motion have been discussed above. However, the storm was at the short end of the spectrum of supercell lifetimes. The parent storm had existed for over an hour before the storm split and rotation developed within the left-moving storm, but the rotation and apparent supercell organization was relatively short lived. An anticyclonic mesovortex and other supercell signatures were present for only a half hour or so, and maximum rotational velocities reached only about 15 m s^{-1}. While other interpretations are possible, we therefore choose to classify this storm as a marginal supercell thunderstorm, of a type which Browning (1968, 1990) calls SL, for severe left mover.

No hook or bounded weak echo region, which would be indicators of a strong supercell thunderstorm, were evident in this storm. Many supercell thunderstorms lack these two features (Bluestein 1993), and it is not surprising that they were missing in this relatively weak, short-lived supercell. It is also possible that a hook or a bounded weak echo region was present but was not detected because of the width of the radar beam at this range. At a distance of 120–140 km, the one-way 3-

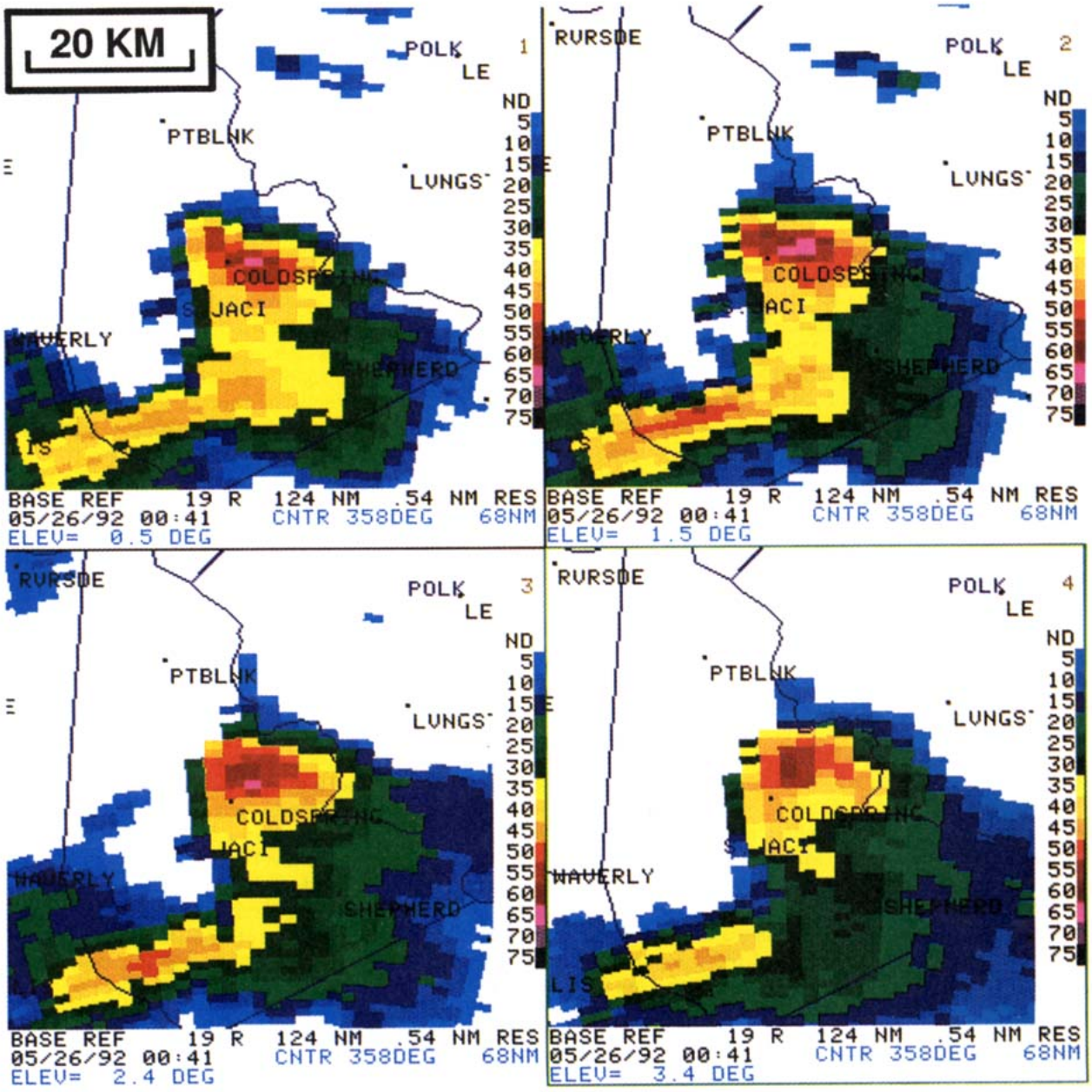

FIG. 10. Four-panel base reflectivity fields centered on the left-moving thunderstorm, 0041 UTC 26 May 1993 (6 min after Fig. 9). Data from the lowest four elevation angles are shown. The radar is located 126 km south of the center of each panel. Reflectivity scales (on right) are in dBZ.

dB beamwidth of 0.95° (Crum and Alberty 1993) corresponds to a physical beamwidth of between 2 and 2.3 km.

d. The flare echo

The reflectivity pattern also shows a protrusion of weak echo north of the core of strongest reflectivity. These protrusions are observed at other times as well (see Fig. 13), and are found only along radials that pass through the reflectivity core of the Coldspring storm when the maximum reflectivity of the core is 58 dBZ or greater. Furthermore, the protrusions are longer at higher elevation angles, are longer at a given elevation angle when the core reflectivity is higher, and possess reflectivities that decrease gradually away from the radar. Protrusions possessing these characteristics are called flares (Wilson and Reum 1988, hereafter WR) or hail spikes (Wilson and Reum 1986).

A flare, depicted schematically in Fig. 11, is believed to be produced when the radar beam is scattered downward by water-coated hailstones or other large hydrometeors, scattered back off the underlying land surface, and finally scattered off the hydrometeors again back toward the radar (Zrnić 1987). Because the beam path covers a larger distance than in the case of simple backscattering by the hydrometeors, the return is delayed and appears to be originating from beyond the storm. The flare has much lower intensity than the direct return from the storm, and the reflectivity decreases with increasing distance from the originating reflectivity core. A survey by WR found that flares in Colorado thunderstorms were generally produced by hail, while flares in summertime thunderstorms in northern Alabama were apparently produced by large raindrops. A comparison of flares with maximum reflectivities for this storm revealed that peak reflectivities of at least 58 dBZ produced flares, with the largest flares occurring with the largest reflectivities, 65–67 dBZ. As noted below, this storm was confirmed to contain large hail, and in the following discussion, this flare will be assumed to have been produced by hailstones.

Wilson and Reum performed several tests of the reflectivity and velocity signals within flares in order to confirm consistency with Zrnić's (1987) theory of flare formation. Such tests would be useful here as additional confirmation that this flare was produced by a process such as that shown in Fig. 11. Unfortunately, our ability to perform such tests is limited by our dataset, which consists only of WSR-88D products. One very strict test that can be performed is to examine the location of maximum reflectivity within the flare. According to the theory of Zrnić, the maximum reflectivity should be located at the beginning of the flare, at a distance from the reflectivity core equal to the height of the core above the ground. Wilson and Reum (1986) confirmed this characteristic in all cases which they examined in detail.

In the Coldspring storm, 13 radials were found in which a reflectivity maximum occurred within the flare, displaced from the main body of the storm. For each of these radials, the height of the reflectivity core above the ground was recorded, and the distance from the maximum reflectivity within the core to the maximum reflectivity within the flare was estimated. These latter estimates consist of a range of possible distances, primarily because it is not possible to determine which of several identically colored plotted bins possess the largest reflectivity. The data are plotted in Fig. 12, along with a line representing equal core height and flare distance. Excluding random noise and additional targets within the range of the flare, theory predicts that the core height and flare distance should be equal, and Fig. 12 shows that 12 of 13 computed distances are in agreement with this prediction. The mean difference between the flare distance and the predicted flare distance is −0.2 km, with a standard deviation of 1.0 km. This close agreement supports the conclusion that these features are flares produced by scattering from the earth's surface.

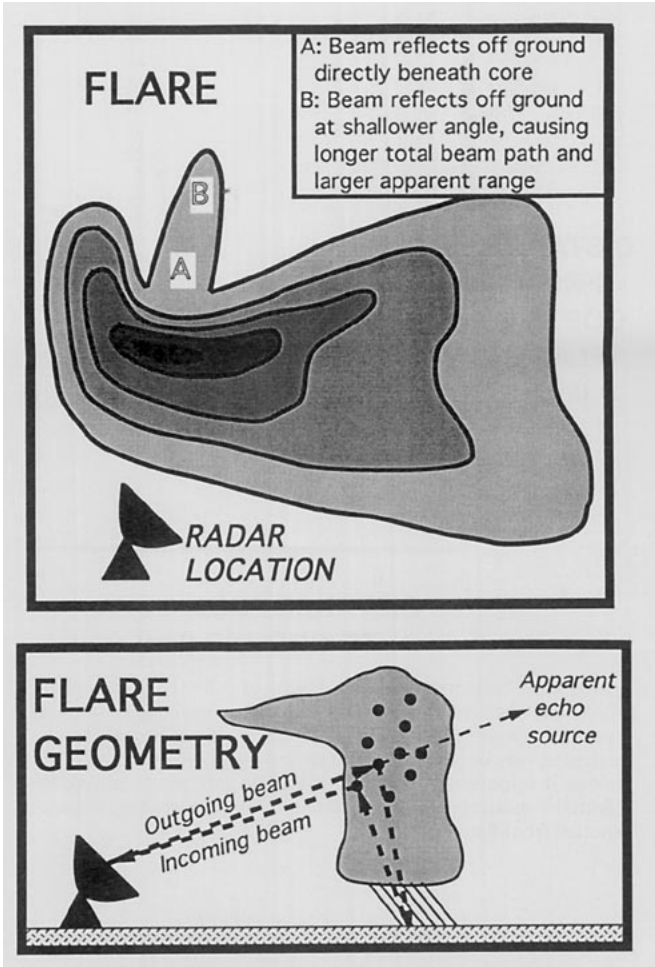

FIG. 11. Schematic diagrams showing the ray path responsible for the generation of a flare and the resulting reflectivity pattern.

Wilson and Reum note that flares are much more commonly observed on 3- and 5-cm radars than on 10-cm radars. However, the WSR-88D radars are horizontally polarized (Crum and Alberty 1993), and according to Wilson (1993, personal communication), flares are more common on horizontally polarized radars than on radars with other polarizations. To our knowledge, no survey has been performed of flares detected by the WSR-88D. This flare, and probably many others, would not appear on a reflectivity display if the display is thresholded to display only reflectivities above 15 dBZ.

Doppler velocities within a flare are biased from true radial velocities by an amount that depends upon the vertical velocity of the hydrometeors and the distance along the flare (Zrnić 1987; WR). The observed Doppler radial velocity V should be approximately equal to

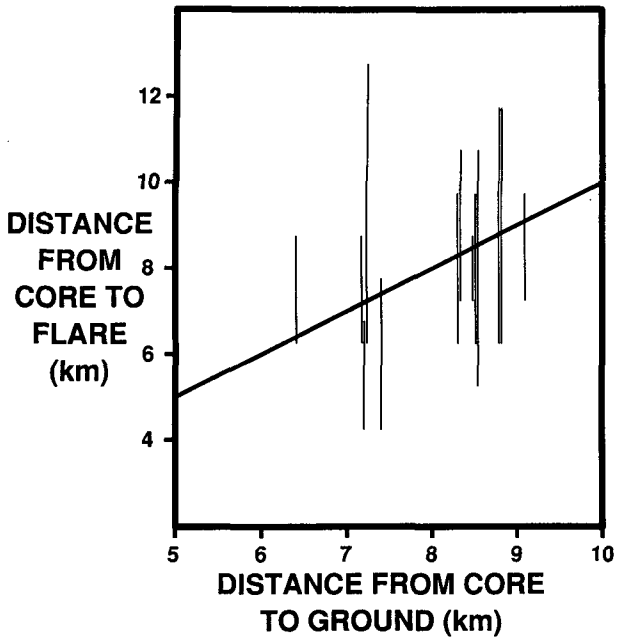

FIG. 12. Comparison between height of reflectivity core above ground and observed distance from reflectivity core to flare reflectivity maximum. Observed distances are plotted as ranges because several range gates may be plotted with the same color in WSR-88D products, making it impossible to identify a specific gate as containing the reflectivity maximum. Diagonal line indicates core-to-flare distance expected from flare theory.

$$V \approx v_r + (w + w_T)H/l,$$

where v_r is the true radial velocity, w is the vertical motion of the air, w_T is the terminal velocity of the hydrometeors, H is the height of the scatterers above the ground, and l is the distance from the flare to the scatterers. For falling hailstones, the flare will usually have a radial velocity bias toward the radar (relative to the rest of the storm), with the largest velocity bias at the base of the flare, closest to the storm.

The Coldspring storm appears to be the first documented case of a flare emanating from a distinct mesovortex. The hail in the Coldspring storm was embedded in strong anticyclonic rotation, so that the left side of the hail core (when viewed by the radar) had Doppler velocities away from the radar while the right side of the hail core had Doppler velocities toward the radar. When the bias due to falling hailstones is included, a flare emanating from an anticyclonically rotating core would be expected to have near-zero Doppler velocities along its left edge and very strong approaching velocities along its right edge, particularly near the base of the flare. This velocity pattern is found repeatedly within the Coldspring flare. In Fig. 9, the 2.4° scan shows maximum measured Doppler velocities greater than 50 kt (>26 m s^{-1}) at the right base of the flare, apparently a combination of approaching velocities of about 26 kt (13 m s^{-1}) within the right side of the anticyclone and hailstone fall velocities of greater than 24 kt (12 m s^{-1}). These fall velocities are a combination of the vertical motion of the air and the terminal velocity of the hailstones. Similar fall velocities have been estimated by WR for other flares.

e. Life cycle of the Coldspring storm

As seen in a time sequence of plan-position indicator (PPI) displays (Fig. 13), the Coldspring storm first became distinct from its parent storm at 0012. To show a consistent evolution of the radial velocity fields, Fig. 13 shows true radial velocities rather than the storm-relative velocities of Fig. 9. By 0018 (not shown), a mesocyclone signature could be seen in both the 2.4° and 3.4° scans (6.0–8.0 km AGL, at a range of 120 km). Through 0059, evidence of anticyclonic rotation persisted at 2.4°. (The flare also bears the signature of anticyclonic rotation during this period.) At this elevation angle, peak reflectivity values of 67 dBZ were observed twice, at 0035 and 0053 (not shown). This double peak was observed at lower elevation angles as well, except that the reflectivity peaks at 1.5° lagged the peaks at 2.4° by 5 min, and the peaks at 0.5° lagged the peaks at 2.4° by 5–10 min. Apparently, the storm involved two strong updrafts 20 min apart. The first reflectivity peak at 3.4° was also 67 dBZ, but the 3.4° reflectivity was only 58 dBZ at 0053, the time of the second maximum at 2.4°, suggesting that the second updraft did not penetrate as high into the storm. (At this range, 135 km, 2.4° corresponds to 6.8 km AGL and 3.4° corresponds to 9.2 km AGL.) Evidence of this change in the storm's structure is also found in the velocity fields; rotation was clearly apparent at 3.4° only between 0018 and 0035.

At 0059, the storm began collapsing: the reflectivity at 3.4° dropped from 57 dBZ to less than 50 dBZ between 0059 and 0104; by 0110, the maximum reflectivity at 3.4° was less than 40 dBZ. The maximum reflectivity at 2.4° fell from 59 dBZ to less than 50 dBZ between 0104 and 0110, lagging the drop higher in the storm by a few minutes. At 0110 the reflectivity at lower elevation angles was still 60 dBZ and higher, but decreased rapidly during the next few minutes (not shown). Furthermore, the Doppler velocities show a decrease in rotation, although they become difficult to interpret at 0110 and beyond because of range-obscured data (coded as purple) in the area of interest. The reason for the lack of additional high-reflectivity episodes in the Coldspring storm may have been the rapid formation of other convective cells in the inflow region to its north, which would have had the effect of cooling the boundary layer and reducing the amount of instability aloft.

The collapse of the reflectivity core after 0059 was apparently accompanied by hail at the surface. Following receipt of the report of wind damage from the Coldspring storm at 0105, the Houston Area WSO is-

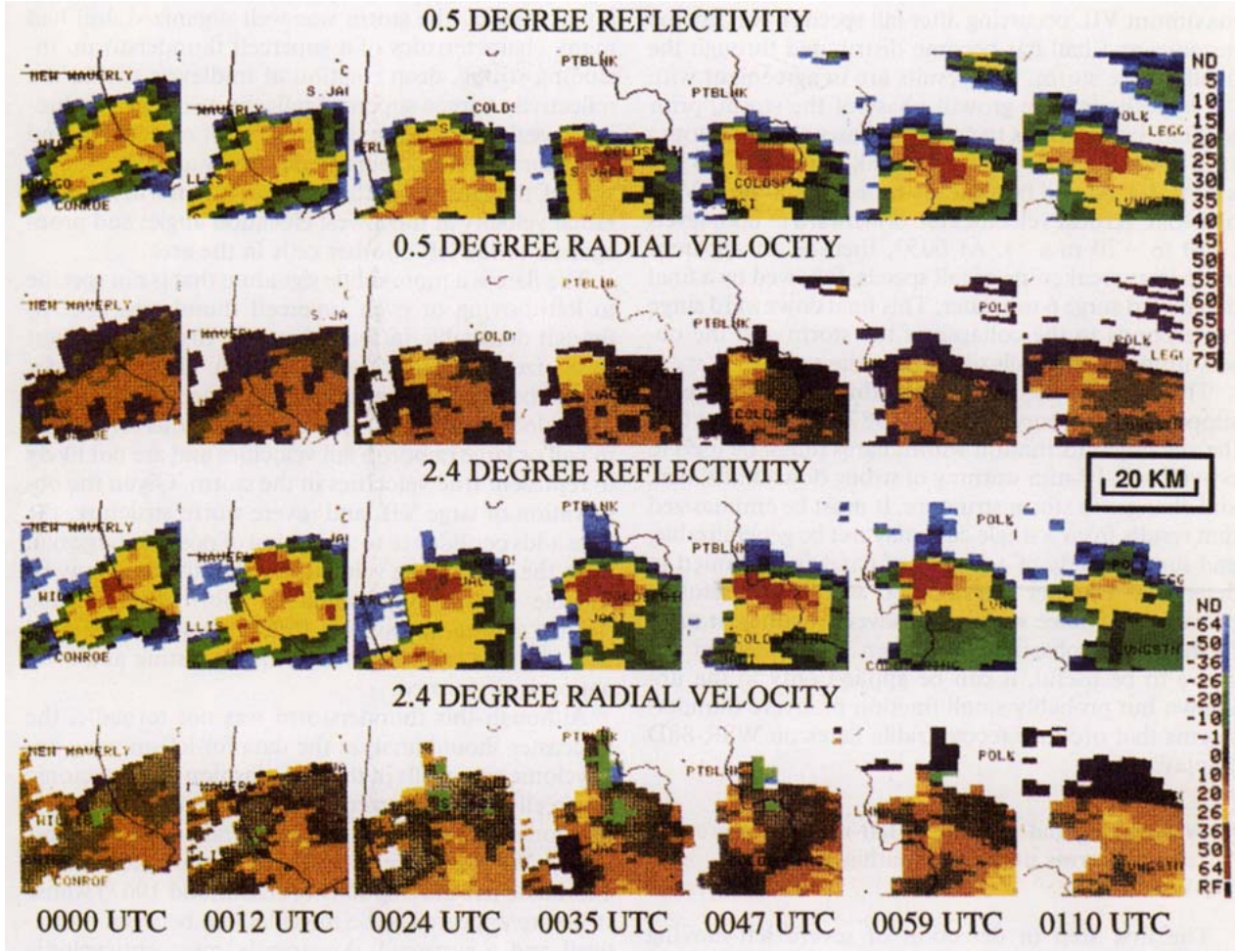

FIG. 13. Sequence of scans showing the evolution of, from top, the low-level reflectivity, the low-level velocity, the midlevel reflectivity, and the midlevel velocity of the left-moving supercell. Each frame is centered on the position of the hypothetical storm moving with uniform velocity that most closely approximates the track and speed of the actual supercell. Reflectivity and velocity scales (on right) are as in Figs. 9 and 10.

sued a severe thunderstorm warning for Polk County. At 0130 the WSO received a report from the Polk County sheriff of golf ball–size hail just west of Livingston. The Coldspring storm was west of Livingston between 0053 and 0110, suggesting that the hail occurred within that time period.

f. Severe weather prediction using Doppler velocities within flares

Wilson and Reum suggest that the downward velocity information contained within flares could be utilized in very short range forecasting of hail and microbursts. To see whether this information could have been utilized in this case for warnings of severe weather, a simple algorithm was developed to estimate fall velocities from WSR-88D products. The first steps in the algorithm are to identify those 1-km-long range bins with the highest plotted reflectivity, to select the most centrally located range bin within the highest-reflectivity field if two or more range bins are plotted with the same high reflectivity, and to record the Doppler radial velocity at that location. Then, along the same radial, the largest inbound Doppler radial velocity within the flare (or smallest outbound, if no inbound velocities are present) is identified and recorded. Finally, the first velocity is subtracted from the second to yield an estimate of the vertical velocity of the hailstones. Positive (upward) or near-zero hailstone vertical velocities would imply hail that is growing in size, while negative (downward) vertical velocities would imply that the hail is descending toward the ground. A rapid transition from upward to downward vertical velocities would, according to WR's hypothesis, indicate the possible initiation of a microburst.

Hailstone vertical velocities were estimated from the 2.4° and 3.4° scan angles using this algorithm, and the estimates are compared with maximum VIL in Fig. 8. Our hypothesis is that upward or near-zero vertical velocities should correspond to increasing VIL, with

maximum VIL occurring after fall speeds have become negative and hail has become distributed through the depth of the storm. The results are in agreement with the hypothesis. The growth phase of the storm, prior to 0030, corresponds to computed ascent of hailstones at 3.4° (8–8.5 km AGL) and weak descent at 2.4° (6 km AGL). At and beyond the time of maximum VIL, hailstone vertical velocities are downward at both levels (-10 to -20 m s^{-1}). At 0053, there is an apparent temporary weakening of fall speeds, followed by a final downward surge 6 min later. This final downward surge corresponds to the collapse of the storm and the observations of golf ball–size hail at the surface.

This simple test provides additional evidence in support of the theory of Zrnić (1987) and suggests that the velocity information within flares might be used to provide a 5–10-min warning of strong downdrafts, hail, and changes in storm structure. It must be emphasized that results from a single case may not be generalizable, and further study of a variety of flares is warranted to determine whether this method would be useful in providing advance warning of severe weather. It must further be emphasized that, even if the method did prove to be useful, it can be applied only to the unknown but probably small fraction of severe thunderstorms that produce recognizable flares on WSR-88D displays.

4. Nowcasting and warning of left-moving severe thunderstorms using information from the WSR-88D

The first step in detection of severe left-moving thunderstorms is awareness that such thunderstorms might form. The forecaster should be aware of the shape and configuration of the hodograph throughout the area in which thunderstorms might form, and should monitor changes in hodograph structure closely. If the hodograph is nearly straight or curves to the left with height, anticyclonically rotating thunderstorms are possible.

Forecaster awareness is also crucial for radar identification of severe left movers. None of the algorithm-derived products that use velocity information are designed to identify anticyclonic rotation. The forecaster must rely on analyses of primarily base products, or "near-base" products such as storm-relative radial velocities, to identify and warn for severe left-moving thunderstorms.

The use of VIL and analyses of storm structure from base reflectivity slices provided the forecaster on duty with sufficient information to issue a warning in advance of observed severe weather for the Coldspring storm. Use of other data, such as time lapse to identify the left-moving character of the storm and recognition of the anticyclonic velocity couplets in the midlevels of the storm, would have provided the forecaster with even more confidence in the warning. During its most intense phase, the storm was well organized and had many characteristics of a supercell thunderstorm, including strong, deep rotation at midlevels within the reflectivity core; a supercell reflectivity pattern including a weak echo region, large values of reflectivity, and large horizontal gradients of reflectivity along the inflow side of the storm (in this case, to the north); strong radial velocity at the lowest elevation angle; and propagation to the left of other cells in the area.

The flare is a more subtle signature that is not specific to left-moving or even supercell thunderstorms. Although detectable in the reflectivity display, it is best recognized in the velocity pattern. The forecaster should be able to discern that the apparent large shears and velocities are a result of the anomalous return due to hail or large raindrop fall velocities and are not likely to represent true velocities in the storm. Given the observation of large VIL and severe storm structure, the flare adds confidence to a warning of possible large hail from the storm. The velocities within the flare may be capable of providing valuable information on the storm's evolution, but this technique should be used with extreme caution until adequate testing and evaluation is performed.

Although this thunderstorm was not tornadic, the forecaster should analyze the data for left-moving anticyclonic supercells in the same fashion as for cyclonic supercells. The occurrence of a tornado from an anticyclonic supercell is an extremely rare event (Burgess 1981). We are aware of only one documented case of a tornadic left-moving storm (Hammond 1967) whose structure appeared to be intermediate between a multicell and a supercell. Apparently most anticyclonic tornadoes occur in conjunction with cyclonic tornadoes and are not likely to be associated with an anticyclonic mesocyclone (Cotton and Anthes 1989; Fujita 1977). Davies-Jones (1986) proposes that the apparent lack of tornadoes associated with anticyclonic supercells is due to the frictionally induced ground-relative veering of environmental winds near the surface.

As experience with the WSR-88D grows nationwide, the number of confirmed cases of anticyclonic supercells will increase, as witnessed by two recent reports of severe anticyclonic supercell thunderstorms (Andra 1993; Kleyla 1993). Such supercells may prove to be relatively frequent in areas of the country where environmentally favorable wind profiles develop more frequently, including stationary subtropical frontal zones, topographically forced winds (Cotton et al. 1982; Tripoli and Cotton 1986; Houze et al. 1993), and mature sea–lake breeze circulations.

This event occurred shortly after installation of the Houston Area WSR-88D. The forecasters on duty were working their first severe weather event using the new radar. While warnings issued were adequate, greater experience might have given the forecasters enough confidence to issue warnings with greater lead time and

for counties downstream without relying on ground truth.

5. Summary

This paper documents the life cycle of a rare anticyclonically rotating severe thunderstorm observed by the WSR-88D at the Houston Area WSO at League City, Texas, on 26 May 1992. The thunderstorm produced damaging winds and golf ball–size hail. Because anticyclonic mesocyclones are not flagged by the WSR-88D mesocyclone algorithm, because forecasters are less familiar with left-moving thunderstorms, and because left-moving thunderstorms are not necessarily severe or supercellular (cf. Houze et al. 1993), this paper notes radar-detectable features of the storm that should help forecasters to manually identify and warn for severe anticyclonic supercells.

One cannot conclude from this case study that the WSR-88D mesocyclone detection algorithm should be expanded to include the capability of detecting mesoanticyclones. Assuming that the conditions that produce false alarms have equal probabilities of producing signatures with cyclonic or anticyclonic shear, the present algorithm eliminates half of all possible false alarms while excluding only the small fraction of mesovortices that are anticyclonic. A more extensive study would be needed to determine whether the increased detection rate associated with a mesoanticyclone algorithm is worth the computer processing time and the expected increase in the false alarm rate.

Another noteworthy feature associated with this severe thunderstorm was the flare. The value of a flare as a possible indicator of hail within the storm must be determined locally and by season, given the differences found by WR between Colorado and Alabama flares. We have shown that the use of vertical velocities deduced from flares may have the potential to improve the lead time of severe weather warnings in some cases, but considerable testing and evaluation under a variety of conditions is necessary before it is known whether such a technique would be reliable or generally useful.

Acknowledgments. We are grateful for discussions and suggestions from Peter Neilley, James Wilson, and Lyn Neilley, and editing by Elizabeth Nielsen–Gammon. Rawinsonde data in SHARP format and valuable suggestions for improving the manuscript were kindly provided by Steve Keighton. This work was supported by the Partner's Program of the University Corporation for Atmospheric Research's Cooperative Program for Meteorology, Education and Training, and by the National Weather Service.

REFERENCES

Alberty, R. L., 1993: An update on the NEXRAD program and examples of recent WSR-88D successes. Preprints, *26th Int. Conf. on Radar Meteorology,* Norman, OK, Amer. Meteor. Soc., 5–7.

Andra, D. L., Jr., 1993: Observations of an anticyclonically rotating severe storm. Preprints, *17th Conf. on Severe Local Storms,* St. Louis, MO, Amer. Meteor. Soc., 186–190.

Bluestein, H. B., 1993: *Synoptic–Dynamic Meteorology in Midlatitudes.* Vol. 2. *Observations and Theory of Weather Systems.* Oxford University Press, 594 pp.

Brandes, E. A., 1984: Vertical vorticity generation and mesocyclone sustenance in tornadic thunderstorms: The observational evidence. *Mon. Wea. Rev.,* **112,** 2253–2269.

Brown, R. A., and V. T. Wood, 1991: On the interpretation of single-Doppler velocity patterns within severe thunderstorms. *Wea. Forecasting,* **6,** 32–48.

Browning, K. A., 1968: The organization of severe local storms. *Weather,* **23,** 429–434.

——, 1990: Organization and internal structure of synoptic and mesoscale precipitation systems in midlatitudes. *Radar in Meteorology,* D. Atlas, Ed., Amer. Meteor. Soc., 433–460.

Burgess, D. W., 1976: Single-Doppler radar vortex recognition. Part I: Mesocyclone signatures. Preprints, *17th Conf. on Radar Meteorology,* Seattle, WA, Amer. Meteor. Soc., 97–103.

——, 1981: Evidence for anticyclonic rotation in left-moving thunderstorms. Preprints, *20th Conf. on Radar Meteorology,* Boston, MA, Amer. Meteor. Soc., 52–54.

Cotton, W. R., and R. A. Anthes, 1989: *Storm and Cloud Dynamics.* Academic Press, 883 pp.

——, R. L. George, and K. R. Knupp, 1982: An intense, quasi-stationary thunderstorm over mountainous terrain. Part I: Evolution of the storm-initiating mesoscale circulation. *J. Atmos. Sci.,* **39,** 328–342.

Crum, T. D., and R. L. Alberty, 1993: The WSR-88D and the WSR-88D Operational Support Facility. *Bull. Amer. Meteor. Soc.,* **74,** 1669–1688.

Davies-Jones, R. P., 1984: Streamwise vorticity: The origin of updraft rotation in supercell storms. *J. Atmos. Sci.,* **41,** 2991–3006.

——, 1986: Tornado dynamics. *Thunderstorm Morphology and Dynamics.* 2d ed. E. Kessler, Ed., University of Oklahoma Press, 197–236.

——, D. W. Burgess, and M. Foster, 1990: Test of helicity as a forecast parameter. Preprints, *16th Conf. on Severe Local Storms,* Kananaskis Park, AB, Canada, Amer. Meteor. Soc., 588–592.

Donaldson, R. J., Jr., 1970: Vortex signature recognition by Doppler radar. *J. Appl. Meteor.,* **9,** 661–670.

Doswell, C. A., III, and D. W. Burgess, 1993: Tornadoes and tornadic storms: A review of conceptual models. *The Tornado: Its Structure, Dynamics, Prediction, and Hazards,* C. Church, D. Burgess, C. Doswell, and R. Davies-Jones, Eds., American Geophysical Union Press, 161–172.

Droegemeier, K. K., S. M. Lazarus, and R. P. Davies-Jones, 1993: The influence of helicity on numerically simulated convective storms. *Mon. Wea. Rev.,* **121,** 2005–2029.

Federal Meteorological Handbook, 1990: Doppler radar meteorological observations, Part C, WSR-88D products and algorithms. FCM-H11C-1991, Interim Version One, Office of the Federal Coordinator for Meteorological Services and Supporting Research, Rockville, Maryland, 210 pp.

Forbes, G. S., 1981: On the reliability of hook echoes as tornado indicators. *Mon. Wea. Rev.,* **109,** 1457–1466.

Fujita, T. T., 1977: Anticyclonic tornadoes. *Weatherwise,* **30,** 51–64.

Greene, D. R., and R. A. Clark, 1972: Vertically integrated liquid water—A new analysis tool. *Mon. Wea. Rev.,* **100,** 548–552.

Hammond, G. R., 1967: Study of a left moving thunderstorm of 23 April 1964. ESSA Tech. Memo. IERTM-NSSL-31, Norman, OK, 75 pp. [Available from the National Severe Storms Laboratory, 1313 Halley Circle, Norman, OK 73069.]

Houze, R. A., Jr., W. Schmid, R. G. Fovell, and H.-H. Schiesser, 1993: Hailstorms in Switzerland: Left movers, right movers, and false hooks. *Mon. Wea. Rev.,* **121,** 3345–3370.

Klazura, G. E., and D. A. Imy, 1993: A description of the initial set of analysis products available from the NEXRAD WSR-88D system. *Bull. Amer. Meteor. Soc.,* **74,** 1293–1311.

Klemp, J. B., and R. B. Wilhelmson, 1978: Simulations of right- and left-moving storms produced through storm splitting. *J. Atmos. Sci.*, **35**, 1097–1110.

Kleyla, R. P., 1993: A radar and synoptic scale analysis of a splitting thunderstorm over north-central Texas on November 10, 1992. Preprints, *17th Conf. on Severe Local Storms*, St. Louis, MO, Amer. Meteor. Soc., 211–213.

Knupp, K. R., and W. R. Cotton, 1982a: An intense, quasi-steady thunderstorm over mountainous terrain. Part II: Doppler radar observations of the storm morphological structure. *J. Atmos. Sci.*, **39**, 343–358.

——, and ——, 1982b: An intense, quasi-steady thunderstorm over mountainous terrain. Part III: Doppler radar observations of the turbulent structure. *J. Atmos. Sci.*, **39**, 359–368.

Koch, S. E., M. desJardins, and P. J. Kocin, 1983: An interactive Barnes objective map analysis scheme for use with satellite and conventional data. *J. Climate Appl. Meteor.*, **22**, 1487–1503.

Lemon, L. R., and C. A. Doswell III, 1979: Severe thunderstorm evolution and mesocyclone structure as related to tornadogenesis. *Mon. Wea. Rev.*, **107**, 1184–1197.

Mahoney, E. A., and R. Schaar, 1993: WSR-88D scan strategy impacts on the vertically integrated liquid product. Preprints, *26th Int. Conf. on Radar Meteorology*, Norman, OK, Amer. Meteor. Soc., 44–46.

Ray, P., 1990: Convective dynamics. *Radar in Meteorology*, D. Atlas, Ed., Amer. Meteor. Soc., 348–390.

Rotunno, R., 1981: On the evolution of thunderstorm rotation. *Mon. Wea. Rev.*, **109**, 577–586.

Tripoli, G. J., and W. R. Cotton, 1986: An intense, quasi-steady thunderstorm over mountainous terrain. Part IV: Three-dimensional numerical simulation. *J. Atmos. Sci.*, **43**, 894–912.

Weisman, M. L., and J. B. Klemp, 1982: The dependence of numerically simulated convective storms on vertical wind shear and buoyancy. *Mon. Wea. Rev.*, **110**, 504–520.

——, and ——, 1986: Characteristics of isolated convective storms. *Mesoscale Meteorology and Forecasting*, P. Ray, Ed., Amer. Meteor. Soc., 331–358.

Wilson, J. W., and D. Reum, 1986: "The Hail Spike": Reflectivity and velocity signature. Preprints, *23d Conf. on Radar Meteorology*, Snowmass, CO, Amer. Meteor. Soc., R62–R65.

——, and ——, 1988: The flare echo: Reflectivity and velocity signature. *J. Atmos. Oceanic Technol.*, **5**, 197–205.

Winston, H. A., and L. J. Ruthi, 1986: Evaluation of RADAP II severe-storm detection algorithms. *Bull. Amer. Meteor. Soc.*, **67**, 145–150.

——, and E. N. Rasmussen, 1989: A study of various implementations of the NEXRAD VIL algorithm. Preprints, *24th Conf. on Radar Meteorology*, Tallahassee, FL, Amer. Meteor. Soc., 232–235.

Zrnić, D. S., 1987: Three-body scattering produces precipitation signature of special diagnostic value. *Radio Sci.*, **22**, 76–86.

——, D. W. Burgess, and L. D. Hennington, 1985: Automatic detection of mesocyclonic shear with Doppler radar. *J. Atmos. Oceanic Technol.*, **2**, 425–438.